Chapter 10
Zn Distribution and Chemical Speciation in Marine Biominerals: An Example on Bivalve and Foraminifera Shells from Polluted Sites

Giovanni De Giudici, Carlo Meneghini, Carla Buosi, Ilaria Carlomagno, Giuliana Aquilanti, Tohru Araki, Diana E. Bedolla, Maria Antonietta Casu, Antonietta Cherchi, Alessandra Gianoncelli, Antonella Iadecola, Andrei C. Kuncser, V. Adrian Maraloiu, Olivier Mathon, Valentina Rimondi, Pierpaolo Zuddas, and Daniela Medas

Abstract Biominerals are widespread in Nature and they precipitate to respond to different physiological purposes. A broad knowledge of their chemical and structural properties offers a unique opportunity to improve our capability to reconstruct actual and paleoenvironment. In this work, we show two case studies, bivalves and foraminifera grown in polluted sites that were characterized by applying different

G. De Giudici · C. Buosi · A. Cherchi · D. Medas (✉)
Department of Chemical and Geological Sciences, University of Cagliari, Cagliari, Italy
e-mail: dmedas@unica.it

C. Meneghini
Department of Sciences, University of Roma Tre, Rome, Italy

I. Carlomagno · G. Aquilanti · D. E. Bedolla · A. Gianoncelli
Elettra-Sincrotrone Trieste, Basovizza, Trieste, Italy

T. Araki
Diamond Light Source, Diamond House, Harwell Science and Innovation Campus, Oxfordshire, Didcot, UK

M. A. Casu
Institute of Translational Pharmacology, Scientific and Technological Park of Sardinia POLARIS, UOS of Cagliari, National Research Council, Pula, Italy

A. Iadecola
RS2E, Réseau Français Sur Le Stockage Electrochimique de L'Energie, Amiens, France

A. C. Kuncser · V. A. Maraloiu
Laboratory of Atomic Structures and Defects in Advanced Materials, National Institute of Materials Physics, Magurele, Romania

O. Mathon
The European Synchrotron Radiation Facility (ESRF), Grenoble, France

V. Rimondi
Department of Earth Sciences, University of Florence, Florence, Italy

CNR—Institute of Geosciences and Earth Resources, Florence, Italy

A. Di Cicco et al. (eds.), *Synchrotron Radiation Science and Applications*,
Springer Proceedings in Physics 220, https://doi.org/10.1007/978-3-030-72005-6_10

and complementary synchrotron radiation-based investigation techniques, mainly focused on the investigation of Zn incorporation in the biomineralized shells. Using scanning transmission X-ray microscopy (STXM) and X-ray micro-fluorescence (μ-XRF), we found the colocalization of elements across the shells, while we obtained information on chemical speciation of Zn by applying X-ray absorption spectroscopy (XAS). Noticeably, instead of metal dispersion in the Ca-carbonate shells, we found traces of several independent phases, in particular for Zn, dispersed generally as microscopic minerals. This work provides fundamental insight into the structural properties, coordinative and chemical environment of some marine biominerals. This new knowledge is fundamental to understand the biogeochemical processes and to develop effective environmental proxies.

10.1 Introduction

Biominerals are biogenic composite materials, made up of organic and mineral phases, produced by living organisms for different purposes, such as defense against predators, protection of the vital organs, support of the body, and others [1]. Biominerals are spread everywhere in the biosphere and in the geological record, and often include impurities and defects due to interactions between the organism and the surrounding environment [2–5], therefore they can bring important information about local biogeochemical conditions.

Bivalve and foraminiferal shells, ubiquitous biominerals in modern and paleomarine environments, are often used as environmental proxies [6–9]. Bivalve shells are formed by an extracellular biomineralization made up of different layers, resulting in an organo-mineral biocomposite, where the Ca-carbonate mineral (calcite, aragonite or vaterite, [10]) represents up to 95–99% [11]. The bivalve shell consists of three layers. The outmost one is the periostracum made up of conchiolin, an unmineralized protein layer that covers the external surface of the shell, enhancing abrasion resistance and acting as a barrier against predation. The periostracum provides the nucleation site for calcium carbonate [12]. Below the periostracum grows a prismatic layer that is secreted by the outer mantle fold [13], containing organic matrices consisting of chitin and proteins [14, 15]. Finally, the nacreous layer is deposited; it is a microlaminate composite material with highly oriented aragonite crystals [16]. The organic matrix consists of several macromolecules, polysaccharides and proteins, located in both intercrystalline and intracrystalline positions within the nacre [13].

Foraminifera are mainly marine organisms and can live on the seafloor sediments (i.e., benthic species), or can float in the water column at various depths (i.e., planktonic species) [17]. Foraminifera produce their own shell, characterized either by one or multiple chambers commonly made up of calcium carbonate, through a controlled biomineralization process. Magnesium content is related to the biomineralization

P. Zuddas
Sorbonne Universités, METIS, Paris, France

mechanism. Shells precipitated by Rotaliida through an extracellular biosynthesis are characterized by low-Mg contents, small crystallites and generally a spiral form. Miliolida form their own shell by an intracellular biomineralization mechanism, precipitating calcite inside the cell and extruding crystals externally into an organic matrix. These are characterized by high-Mg contents and have a porcelaneous shell with calcite growing in form of large needle-like crystallites [18].

Bivalve and foraminiferal shells are useful environmental proxies because variations in the shell structure or composition reflect physicochemical variations in the surrounding environment [19–21]. The evolution of the watershed (annual cycles in rainfall and soil erosion and/or sediment inputs) can be understood looking at the trace element profiles of bivalves by laser ablation inductively coupled plasma mass spectrometry (LA ICP-MS) [22]. The measurement of Mg/Ca ratio and Ca isotopes in foraminifera represents a relevant proxy for the evaluation of paleotemperature [21], and B/Ca ratio is used as a paleo-pH proxy to investigate the evolution of the carbonate saturation state in the oceans [2, 23].

Previous literature has shown that bivalves accumulate trace elements from the external environment and that metal detoxification can occur by their deposition in the mineral structures (shell and/or microspherules [24]) leading to structural alterations in the nacreous layer [25]. In foraminifera, morphological deformities were observed both in fossils and in modern specimens, probably in response to environmental stress [26].

Among trace elements, Zn is relevant for natural healthy biochemical processes, and it is an essential nutrient in many phytoplankton enzymes, particularly those of eukaryotes [27], playing an important role in marine primary production. Determination of Zn and other trace or major elements in carbonates allows to develop sensitive proxies to reveal paleocean characteristics. For instance, Liu et al. [28] have demonstrated that Zn/Fe ratio in shallow marine carbonate rocks has potential to provide a quantitative tracer for the long-term redox evolution of the oceans. Also, the Zn/Ca ratio of benthic foraminifera has been successfully used to reconstruct past deep ocean nutrient concentrations, providing insights into the changes in the physical circulation of the ocean through Earth history [4].

Zinc may result toxic in high concentrations originating from natural and/or anthropological contamination sources [29, 30]. Despite the rapid development of the research addressed to trace metals in marine (micro)organisms, the coordination chemistry and mineral speciation of Zn incorporated into the biomineralized shell of bivalve and foraminifera have been over-looked compared to other more harmful elements, though they represent a fundamental knowledge in order to assess the nature of Zn biomineral phases and the biological mechanisms involved in the detoxification. These have important implications to achieve information on the biomineralization mechanism, helpful to understand the biogeochemical processes and to develop effective biomonitoring techniques. In our studies, we have developed a research topic aimed to understand the fate of Zn in foraminiferal and bivalve shells [31, 32] through a multi-technique approach that combines state of the art complementary techniques namely: i) transmission electron microscope (TEM), ii) scanning transmission X-ray microscopy (STXM), and iii) X-ray micro-fluorescence (μ-XRF) to

localize Zn at the micro and nanoscale; iv) X-ray absorption spectroscopy (XAFS) to individuate the Zn coordination chemistry; v) X-ray diffraction (XRD) to identify mineralogic phases. As representative examples, we describe in detail the Zn incorporation in different bivalve genera (*Donax*, *Lentidium* and *Chamelea*) and in the shells belonging to two benthic foraminiferal species (*Elphidium aculeatum* belonging to the Rotaliida order, and *Quinqueloculina seminula* belonging to the Miliolida order), collected from polluted environments. Specifically, bivalves were collected from the abandoned mining site of Malfidano (SW Sardinia, Italy), and foraminifera from La Maddalena Harbour (N Sardinia, Italy), an area characterized by past military activity.

10.2 Investigated Areas and Samples

10.2.1 Bivalve Samples

The Malfidano area is located in the Iglesiente mining district (SW Sardinia, Fig. 10.1a-point 1, and Fig. 10.1b). The main deposits consist of Paleozoic formations represented by Cambrian–Ordovician rocks. The Lower Cambrian successions are made up of siliciclastic sedimentary rocks, carbonate intercalations (Nebida Group) and shallow water platform carbonate rocks (Gonnesa Groups [33]). The Middle and Upper Cambrian–Lower Ordovician successions comprise nodular limestones and slates (Campo Pisano Formation, Iglesias Group). Aeolian dunes along the coast and fluvial deposits in the internal area are the main Quaternary outcrops.

The mine was active from 1870 to 1980, and ore deposits consisted both of primary sulfides, resulting from the metamorphism and magmatism of the Variscan Orogeny [34], and calamine deposits. In the Iglesiente mining district, the primary sulfides included sphalerite (ZnS) and galena (PbS), with a normal Zn grade of about 8–12 wt%, that occurred in columnar, massive, lens- and vein-like shapes in the carbonatic formations [34]. The calamine deposits formed from different weathering events that developed within the Dolomia Gialla (hydrothermal Dolomia Geodica). The principal Zn-bearing minerals were smithsonite ($ZnCO_3$) and hemimorphite ($Zn_4Si_2O_7(OH)_2 \cdot H_2O$), associated with nodules of supergene or remnant galena and sphalerite [35, 36] with an overall Zn grade exceeding 20–22 wt% [34].

In June 2016, bivalve shells of similar sizes were collected from surface sea-bed sediments along Buggerru and San Nicolò beaches (Fig. 10.1a–c). The most abundant genera were *Donax*, *Lentidium* and *Chamelea* (Fig. 10.1d). At least 50 specimens for each genus were collected, immediately stored in bags and transported to the laboratory. About 20 specimens per genus for each beach were selected, polled into one sample and ground for mineralogical investigation, chemical analysis, and XAS analysis.

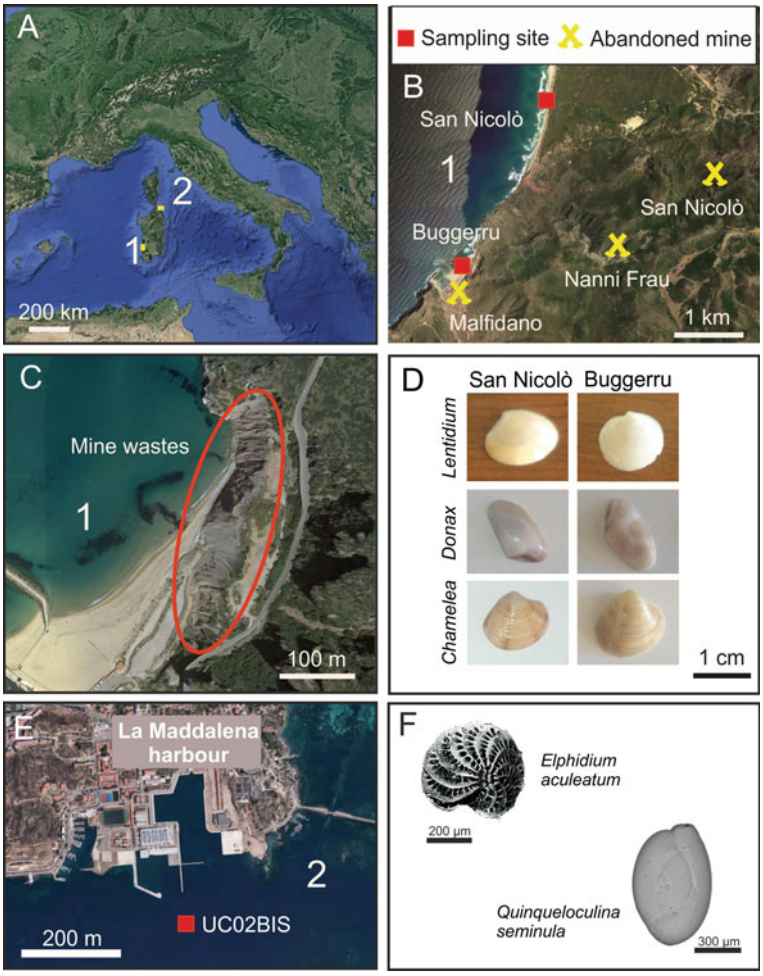

Fig. 10.1 Localization of Sardinia island (**a**); bivalve sampling site (**b**); detail on mining wastes disposed near the Buggerru beach (**c**); selected photos of bivalve genera collected at Buggerru and San Nicolò beaches (**d**); foraminiferal sampling site (**e**), and selected photos of *Elphidium aculeatum* and *Quinqueloculina seminula* collected near the La Maddalena harbor (**f**)

10.2.2 Foraminiferal Samples

La Maddalena Harbour is located in the La Maddalena Island (NE Sardinia; Fig. 10.1a-point 2). This island belongs to the La Maddalena Archipelago. The archipelago, with a surface of about 200 km^2, is characterized by a complex system of inlets, promontories, bays, channels and paleo-fluvial valleys (*rias*) [37]. It represents the uppermost part of the NNE Hercynian plutonic basement, and mainly consists of leucogranites, crossed by a N-S-trending late dyke system.

The La Maddalena Archipelago is minimally affected by intense industrial activity [38], the anthropogenic impact is limited to the La Maddalena and S. Stefano military harbors [38–40]. Specifically, La Maddalena Harbour was devoted to military activities for more than a century, as refined in preparation for the G8 meeting in 2009. The superficial sediments of the La Maddalena Harbour show an enrichment in pollutants such as As, Hg, Zn, Cu, Pb, Cd and hydrocarbons (C > 12), with a maximum concentration of Zn in sediments of around 1600 ppm [40].

Surface sediment samples for the investigation of the Zn incorporation in foraminiferal shells were collected at one station (UC02BIS) from a short core with a length of 3 m in October 2011 (Fig. 10.1e). Only the topmost sediment layer (0–2 cm) was used for analysis. Sediments were preserved in ethanol and Rose of Bengal (2 g of Rose of Bengal in 1000 ml of ethyl alcohol) for foraminiferal recognition [41]. A constant volume of approximately 50 cm^3 was dried at 50 °C and weighed. After drying and sieving the residues on a 63-μm mesh, the foraminifera were examined under a binocular microscope. At least 300 living benthic foraminifera from each sample were picked for micropalaeontological analysis. Benthic foraminifera were identified according to several taxonomic works [42–45]. Specifically, we investigated the Zn coordinative environment in individual tests of two species of benthic foraminifera, *Elphidium aculeatum* (Rotaliida, low-Mg calcite) and *Quinqueloculina seminula* (Miliolida, high-Mg calcite) (Fig. 10.1f).

10.3 Analytical Methods

10.3.1 Bivalve Analysis

Shell samples were washed in laboratory with deionized water and were brushed with a nylon toothbrush to eliminate sand, algae and other impurities. Samples were then washed several times in Milli-Q water and dried at room temperature for one week. Samples were ground in an agate mortar and analyzed by XRD using laboratory θ-θ equipment (Panalytical) with Cu K_α radiation ($\lambda = 1.54060$ Å), operating at 40 kV and 40 mA, and an X′celerator detector.

Acid digestions were performed by EPA method 3050 with slight modifications according to Conners et al. [46]. Zinc and Fe concentrations were quantified by inductively coupled plasma optical emission spectroscopy (ICP-OES, ARL Fisons ICP Analyzer 3520 B), and inductively coupled plasma mass spectrometry (ICP-MS, Perkin-Elmer, Elan 5000/DRC-e, USA). For the acid digestion method, potential contamination, precision and accuracy were evaluated processing blank solutions, duplicate samples and the certified reference material B.C.S. No. 368—dolomite. For ICP-OES and ICP-MS analysis, reference solutions (SRM 1643e and EnviroMAT Drinking Water, High EP-H-3 and Low EP-L-3) were analyzed every five samples to estimate method precision and accuracy.

Zinc and Fe distributions were investigated by scanning transmission X-ray microscope (STXM) at the TwinMic beamline, at Elettra-Sincrotrone Trieste (Trieste, Italy) [47–53] and by Energy-dispersive X-ray spectroscopy transmission electron microscopy (EDS TEM) at the NIMP (Laboratory of Atomic Structures and Defects in Advanced Materials, Magurele, Romania). Calcium and sulfur distributions were further investigated by STXM combined with XRF elemental mapping analysis at the I08-SXM beamline in Diamond Light Source, Didcot, UK (for details in sample preparation and instrument characteristics see Medas et al. [31]). The linear correlation $\rho_{A\text{-}B}$ between the fluorescence intensities of A and B elements in the maps was calculated to evaluate the relative distribution of selected elements in the shells. The correlation analysis was carried out using a python script based on the numpy [54] and scipy [55] libraries.

XAS measurements were carried out at the XAFS beamline of Elettra synchrotron radiation facility (Trieste, Italy [56]) at the Zn K-edge (9.659 keV) to probe the Zn coordination chemistry. The XAFS data analysis was performed in the near edge region (XANES) using the linear combination analysis (LCA) method [57, 58]. High quality XAS spectra were acquired in transmission geometry on a set of Zn reference compounds for sake of comparison and used for LCA, including organic (e.g. Zn malate, Zn citrate, Zn cysteine, etc.) and inorganic (e.g. Zn sulfide—sphalerite, Zn hydroxycarbonate–hydrozincite, Zn phosphate–$Zn_3(PO_4)_2$, etc.) compounds. Zn K-edge raw XAS data were treated following the standard procedure for data treatment, normalization and extraction of structural signal [59].

10.3.2 Foraminiferal Analysis

Foraminiferal specimens were divided in two groups accordingly to the Mg-calcite shell composition: *Elphidium aculeatum* (Rotaliida, low-Mg calcite) and *Q. seminul*a (Miliolida, high-Mg calcite). The low- and high-Mg calcite composition is related to differences in the biomineralization mechanisms: *E. aculeatum* provides the calcite shell from extracellular synthesis, on the contrary *Q. seminula* builds its own shell through intracellular mechanism ([18] and references therein).

The foraminiferal specimens were washed and rinsed three times in ultrasonic bath with ultrapure water for 3 min in order to remove impurities and to avoid the contribution of small sediments grains. Selected foraminiferal shells had been previously investigated by ESEM (environmental scanning electron microscopy) in low-pressure mode for morphological and chemical composition analyses (without any Au or C surface coating). Mineralogical analysis was performed by laboratory XRD as for bivalves.

The Zn K-edge XAS measurements were carried out on bulk samples while Zn K-edge μ-XAS measurements were carried out on single specimens of *E. aculeatum* and *Q. seminula*. Bulk measurements were conducted in fluorescence geometry at the Elettra-XAFS beamline (Trieste-Italy; [56]) on two independent sample sets each one comprising about 50 mg (corresponding to approximately 300 specimens)

of *Elphidium* spp. and *Quinqueloculina* spp. tests belonging to different species. The foraminiferal shells were ground and mixed with cellulose matrix and pressed in order to obtain homogeneous pellets suitable for careful handling. Measurements were carried out keeping the samples at liquid N_2 temperature in a wide energy range (up to 10.640 keV), suitable for extended X-ray absorption fine structure (EXAFS) signal analysis.

The μ-XAS measurements were carried out at the ESRF-BM23 beamline (Grenoble-France; [60]) using a 4 × 4 μm^2 X-ray spot. Each specimen was firstly explored on the basis of fluorescence maps (at 12 keV X-ray beam energy) to individuate the metal distribution (mainly Ca, Fe and Zn). The Zn K-edge μ-XAS data were collected in the near edge (XANES) region (from -100 to 150 eV range around the Zn K-edge) in selected Zn rich spots.

10.4 Results

Investigated bivalve shells are mainly made up of aragonite (Table 10.1) with Zn concentration varying between 2 and 80 mg/kg and the highest values were observed in samples from Buggerru, where mining tailings are dispersed in the marine sediments or near to the beach (Fig. 10.1c). Iron shows variable concentrations in all the analyzed samples (8–30 mg/kg).

Selected representative STXM-XRF maps (TwinMic beamline) of thin cross sections of the bivalve shells are shown in Figs. 10.2a, b. The Pearson linear correlation coefficient ρ_{ij} between i and j fluorescence intensities (i, j = Ca, Zn, Fe) has been calculated to depict the relationship among Zn, Fe and Ca distribution within the shell. Correlation analysis reveal that Zn and Fe are weakly correlated ($\rho_{Zn\text{-}Fe}$ = 0.09–0.15) suggesting that they are located in different phases. Also, Zn and Fe are weakly correlated to Ca ($\rho_{Zn\text{-}Ca}$ = 0.23, $\rho_{Fe\text{-}Ca}$ = 0.08), indicating that Zn and Fe are not homogeneously dispersed in the aragonite matrix but may likely occur in Fe or Zn rich specific phases embedded into the shell matrix [31]. Accordingly, TEM analysis (Fig. 10.3a–f) reveals that Zn and Fe clusters occur in different regions of the aragonite biocomposite matrix, resulting in a low correlation coefficient ($\rho_{Zn\text{-}Fe}$

Table 10.1 List of bivalve samples, sampling locality, mineralogical composition and concentration of Zn and Fe from the Malfidano area

Sample	Locality	Mineralogy	Zn (mg/kg)	Fe (mg/kg)
Donax	San Nicolò	Aragonite	2.5	10
Lentidium	San Nicolò	Aragonite	3.6	10
Chamelea	San Nicolò	Aragonite	8.3	20
Donax	Buggerru	Aragonite	27	7.7
Lentidium	Buggerru	Aragonite	29	20
Chamelea	Buggerru	Aragonite	81	30

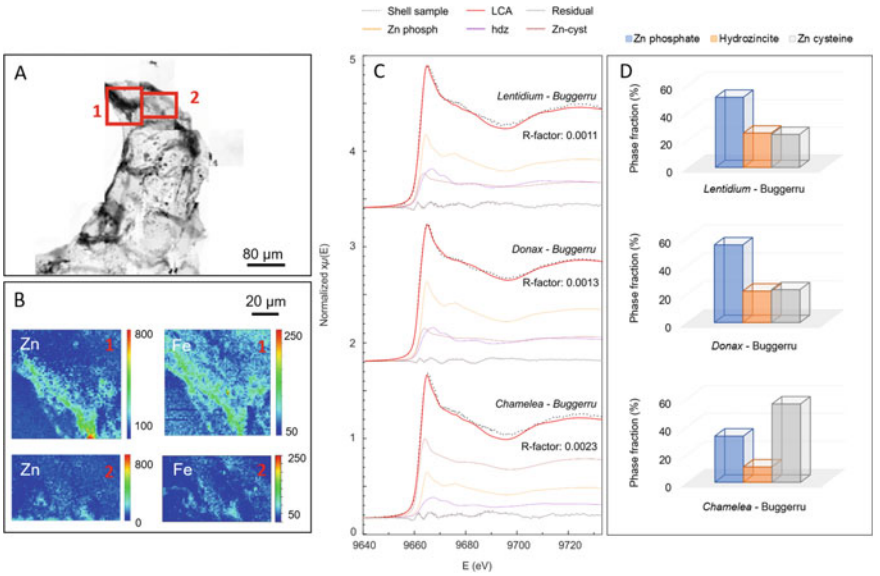

Fig. 10.2 STXM analysis (**a** and **b**) of a selected sample of *Chamelea* collected at Buggerru. Bright field (absorption) image (**a**) and LEXRF maps of Zn and Fe (**b**). Maps 1, size 80 × 80 μm^2, scan 64 × 64 pixels; map 2, size 80 × 40 μm^2, scan 64 × 32 pixels. Linear-combination analysis of the XANES spectra (**c**). Zn phosph (Zn phosphate), hdz (hydrozincite) and Zn-cyst (Zn cysteine). Contribution fractions (sum fixed to 100%) of the Zn phases identified by the LCA (uncertainty around 5–8%) (**d**)

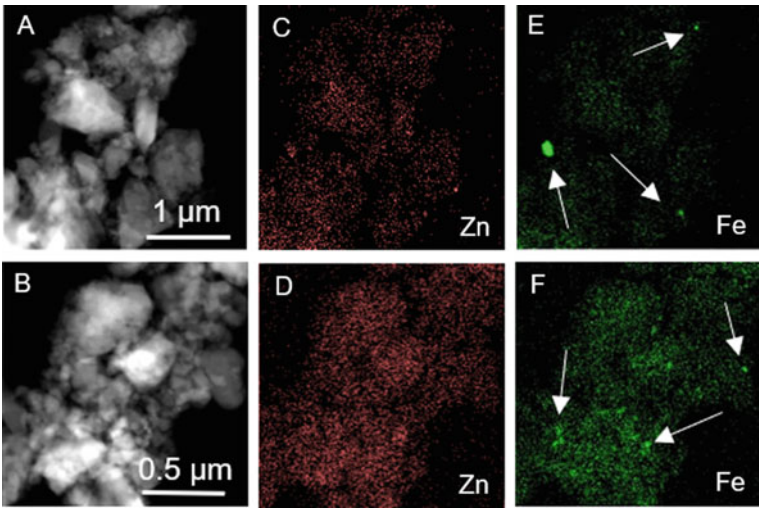

Fig. 10.3 STEM images (**a** and **b**) with the EDS maps of Zn (**c** and **d**) and Fe (**e** and **f**) in bivalve shells. Arrows indicate Fe concentrated spots

= 0.12). Also, Fe can occur as concentrated spots, in agreement with the observed low correlation to Ca ($\rho_{Fe\text{-}Ca} = 0.08$) (for the complete dataset of ρ values see Table 3 in [31]).

Zinc speciation in bivalve shells was investigated by XANES analysis in samples having the highest Zn concentration (*Lentidium*, *Donax* and *Chamelea* from Buggerru). Figure 10.2c shows bivalve shell spectra and the phases identified by the LCA. The XANES spectral features are smoother and broader with respect to the reference compounds, likely due to several Zn-phases and/or disordered Zn coordination environment in the shell samples. Comparing the Zn XANES spectral features of bivalve samples with those of the reference compounds, the similarity with the Zn phosphate spectrum is clear. LCA of XANES spectra was performed to determine the main Zn-phases present in these bivalve samples and the results are shown in Fig. 10.2c–d. In *Lentidium* and *Donax* the main contribution comes from the Zn phosphate (51–55%), followed by hydrozincite (22–25%) and Zn cysteine (23–24%) in similar amount. On the other hand, in *Chamelea*, characterized by the highest Zn content (81 mg/kg) in this study, Zn cysteine (56%) is the most abundant Zn species, followed by Zn phosphate (33%) and hydrozincite (11%), suggesting that cysteine synthesis in the investigated bivalves increases when the Zn uptake from the organism is higher and the excess of Zn is incorporated in the shell as a non-toxic form.

The μ-XRF analysis was used to investigate Ca, Zn and Fe distribution in the foraminiferal shells (Fig. 10.4a). The distribution of Zn and Fe in foraminiferal shells showes clear differences in comparison with bivalve samples. Both Zn and Fe distributions depict spots and inhomogeneities, but Zn appears more broadly diffused in homogeneous halos on the *Q. seminula* specimens. The relatively high correlation between Zn and Fe ρ_{ZnFe} (> 50%) in all samples (up to 70% for *E. aculeatum*) suggests that Fe and Zn tend to be co-located, while the low ρ_{CaFe} (< 15%) in both foraminiferal taxa samples points out the Fe segregation in Fe-rich spots. Interestingly, the correlation between Ca and Zn is largely different in *E. aculeatum* being $\rho_{ZnCa} < 30\%$ and in *Q. seminula* being $\rho_{ZnCa} > 50\%$. This finding quantifies the observation that Zn is mainly localized in *E. aculeatum* while it is more broadly distributed in *Q. seminula* shell.

The analysis of Zn K-edge XAFS spectra from bulk samples revealed a clear structural difference between average Zn environment in *E. aculeatum* and *Q. seminula.* XAFS spectrum of *E. aculeatum* depicts features similar to hydrozincite, whereas *Q. seminula* specimen shows XAFS features of a largely more disordered environment, similar to fourfold-coordinated Zn adsorbed on calcite (Zn_{4c}, see below) (Fig. 10.4b).

Since the μ-XRF data highlighted a nonuniform Zn distribution within the calcite shell, we exploited the μ-XANES as a tool to get further details about the coordination chemistry of Zn in the shells. We collected Zn K-edge μ-XAS spectra at different spots in the samples, characterized by low (L), medium (M) and high (H) normalized fluorescence Zn/Ca intensity ratios R_N (see [32] for details) (Fig. 10.4c), and we exploited the LCA to individuate and quantify the Zn-phases in the shells (Fig. 10.4d). In a preliminary screening among the reference compounds, we found three main Zn containing phases in all the μ-XANES spectra: Zn-hydrozincite, Zn/calcite and Zn_{4C}, the last associated to Zn adsorbed on calcite or hydroxyapatite (the spectra

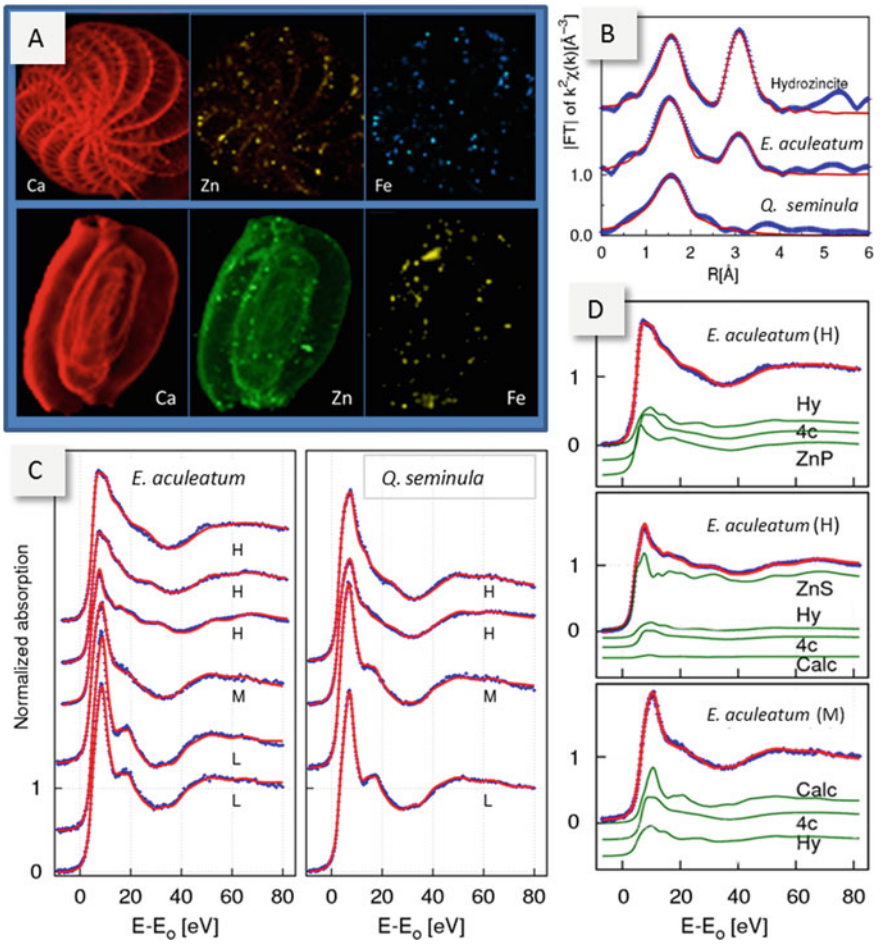

Fig. 10.4 Results of μ-XRF and μ-XANES on foraminifera. μ-XRF maps for *E. aculeatum* (top row) and *Q. seminula* (bottom row) at the Ca, Zn and Fe fluorescence lines (**a**). Moduli of the Fourier Transform (|FT|) of Zn K-edge EXAFS spectra (blue points) measured for hydrozincite mineral reference and bulk samples (about 300 specimens) of *E. aculeatum* and *Q. seminula* (**b**). The |FT| of EXAFS best fit procedures are shown as red lines for completeness. Experimental (blue points) and LCA best fit (red lines) of selected Zn K-edge μ-XANES spectra on *E. aculeatum* (left column) and *Q. seminula* (right column) (**c**). Zn K-edge μ-XANES were measured at selected points in the low (L), medium (M) and high (H) regions of the normalized fluorescence Zn/Ca intensity ratio R_N (see [32] for details). Experimental (blue points) and LCA best fit (red lines) of selected Zn K-edge μ-XANES spectra on *E. aculeatum* (Hy—hydrozincite, 4c—fourfold-coordinated Zn adsorbed, ZnP—$Zn_3(PO_4)_2$, ZnS—sphalerite, Calc—Zn-Ca solid solution) (**d**)

are very similar pointing out very similar Zn adsorption site geometry in calcite and hydroxyapatite).

Our analysis of μ-XANES spectra suggests an intra-specimen variability related to the local Zn concentration. Particularly, high values of the hydrozincite fraction correspond to higher Zn concentration (Zn richer spots, frequent in *E. aculeatum* and rare in *Q. seminula*), while Zn/calcite and Zn_{4C} phases are favored in regions having lower Zn concentration. Moreover, the Zn μ–XANES features also showed the presence of other components such as Zn-sulphide (ZnS) and Zn-phosphate $Zn_3(PO_4)_2$ in some spots of the *Elphidium* spp. samples. Noticeably, further HR-TEM investigation on the same specimens revealed aggregates of Zn carbonate nanocrystals, having an individual size of ~5 nm. Based on the SAED pattern, we identified the main reflections of hydrozincite. In other areas of the *E. aculeatum* shell, we found Zn to be co-located with S, and the SAED pattern revealed the presence of nanocrystalline sphalerite, ZnS, confirming results obtained by μ-XANES analysis.

10.5 Discussion and Conclusions

In our bivalve and foraminifera case-study, we found that large fraction of Zn occurs in independent phases such as Zn-phosphate, Zn-cysteine and even nanocrystalline hydrozincite. Peculiarly, Zn in bivalves does not seems to be incorporated into aragonite lattice or adsorbed onto the surfaces of Ca-carbonate (nano)crystals. This suggests that, under environmental stress, Zn incorporation in bivalve shells occurs with the biosynthesis of phases other than Ca-carbonate. These results point out that bivalves can use different biogeochemical reactions, involving cysteine molecule, phosphate or carbonate ions, to regulate trace element concentrations and their chemical speciation. At the present step of the research, we are not able to assess if these Zn-independent phases were formed as a by-product of the molecular machinery, exploited by the mollusks for the Ca-carbonate synthesis that could be activated also without Zn stress.

This study provided insight into the understanding of cellular control of biomineralization in foraminifera. Combining μ-XRF and μ-XAS techniques, we found that Zn occurs as a solid calcite solution or it is adsorbed onto calcite surfaces and inter-grain spaces due to foraminiferal cellular biosynthesis. Other Zn phases were also detected by XAS and TEM: specifically, hydrozincite was found along with a Zn/Ca solid solution and it is most likely produced during the primary biomineralization process. The occurrence of sphalerite crystals close to calcite aggregates and the presence of detectable amounts of S within the shells, element present in metallothioneins, often used by foraminifera for metal detoxification [61, 62], suggest that sphalerite could be a product of the biosynthesis process but further studies are required to exclude a post-mortem precipitation. Zinc speciation, size of crystal domains and distributions in the shells differ for the two investigated taxa. In calcite needles of *Q. seminula*, Zn is uniformly distributed, and it occurs in a less ordered

environment, indicating that Zn is incorporated more easily during the biologically controlled mineralization processes.

Application of synchrotron techniques such as STXM and μ-XRF to the case-studies allowed us to identify colocalization and chemical distribution of Ca, Zn and Fe across the shells. Moreover, the elemental selectivity and coordination chemistry sensitivity of XAS technique were applied, allowing us to identify the chemical and mineral species of Zn. Understanding biomineralization processes, their structural properties, coordinative and chemical environment offers a unique opportunity to take steps forward in understanding geological record and environmental reconstruction. Paleothermometers and proxies based on elemental ratios and isotopes can be better developed and used when data on microscopic processes and structures are comprised in the models [28]. In this study, we provided relevant information for speciation and location of Fe and Zn in some biominerals. This new knowledge will be of future benefit for the understanding of isotopes fractionation and chemical distribution variability across biomineralization depending on foraminifera and bivalve species.

Acknowledgements We acknowledge CESA (grant number: E58C16000080003) from RAS, and RAS/FBS (grant number: F72F16003080002) grants, the POR FESR Sardegna 2014-2020 (project cluster Top-Down: TESTARE), and the CeSAR (Centro Servizi d'Ateneo per la Ricerca) of the University of Cagliari, Italy, for SEM analysis. The ESRF EV-94 and ES-540 proposals provided access to the BM23 micro-focus experiment. The authors acknowledge the CERIC-ERIC Consortium (grant numbers: 20152020, 20162061, 20167045, 20177041, and 20182100) for the access to experimental facilities and financial support and the Romanian Ministry of Education (through the Core Program, Project PN16-480102). XAFS (Elettra) 20160254 beamtime, Diamond SP16496 beamtime, and grant are acknowledged. The research leading to this result has been supported by the project CALIPSOplus under the Grant Agreement 730872 from the EU Framework Program for Research and Innovation HORIZON 2020. The Grant of Excellence Departments, MIUR (ARTICOLO 1, COMMI 314–337 LEGGE 232/2016), is gratefully acknowledged.

References

1. E. Beniash, Biominerals—hierarchical nanocomposites: the example of bone. Wiley Interdiscip. Rev. Nanomed. Nanobiotechnol. **3**, 47–69 (2011). https://doi.org/10.1002/wnan.105
2. J. Yu, H. Elderfield, Benthic foraminiferal B/Ca ratios reflect deep water carbonate saturation state. Earth Planet. Sci. Lett. **258**, 73–86 (2007). https://doi.org/10.1016/j.epsl.2007.03.025
3. D.W. Lea, G.T. Shen, E.A. Boyle, Coralline barium records temporal variability in equatorial Pacific upwelling. Nature **340**, 373–376 (1989). https://doi.org/10.1038/340373a0
4. S.P. Bryan, T.M. Marchitto, Testing the utility of paleonutrient proxies Cd/Ca and Zn/Ca in benthic foraminifera from thermocline waters. Geochem. Geophys. Geosyst. **11**, Q01005 (2010). https://doi.org/10.1029/2009GC002780
5. A.L. Soldati, D.E. Jacob, P. Glatzel, J.C. Swarbrick, J. Geck, Element substitution by living organisms: the case of manganese in mollusc shell aragonite. Sci. Rep. **6**, 22514 (2016). https://doi.org/10.1038/srep22514
6. L. Chauvaud, A. Lorrain, R.B. Dunbar, Y.-M. Paulet, G. Thouzeau, F. Jean, J.-M. Guarini, D. Mucciarone, Shell of the Great Scallop *Pecten maximus* as a high-frequency archive of paleoenvironmental changes. Geochem. Geophys. Geosyst. **6**, 1–15 (2005). https://doi.org/10.1029/2004GC000890

7. M.H. Klünder, D. Hippler, R. Witbaard, D. Frei, Laser ablation analysis of bivalve shells—archives of environmental information. Geol. Surv. Denmark Greenl. Bull. **15**, 89–92 (2008)
8. A.J. Gooday, Benthic foraminifera (protista) as tools in deep-water palaeoceanography: environmental influences on faunal characteristics. Adv. Mar. Biol. **46**, 1–90 (2003). https://doi.org/10.1016/S0065-2881(03)46002-1
9. E. Armynot du Châtelet, J.-P. Debenay, R. Soulard, Foraminiferal proxies for pollution monitoring in moderately polluted harbors. Environ. Pollut. **127**, 27–40 (2004). https://doi.org/10.1016/S0269-7491(03)00256-2
10. G. Nehrke, H. Poigner, D. Wilhelms-Dick, T. Brey, D. Abele, Coexistence of three calcium carbonate polymorphs in the shell of the Antarctic clam *Laternula elliptica*. Geochem. Geophys. Geosyst. **13**, 1–8 (2012). https://doi.org/10.1029/2011GC003996
11. S. Weiner, H.A. Lowenstam, L. Hood, Characterization of 80-million-year-old mollusk shell proteins. Proc. Natl. Acad. Sci. U. S. A. **73**, 2541–2545 (1976). https://doi.org/10.1073/pnas.73.8.2541
12. A. Checa, A new model for periostracum and shell formation in Unionidae (Bivalvia, Mollusca). Tissue Cell. **32**, 405–416 (2000). https://doi.org/10.1054/tice.2000.0129
13. Z. Yao, M. Xia, H. Li, T. Chen, Y. Ye, H. Zheng, Bivalve shell: not an abundant useless waste but a functional and versatile biomaterial. Crit. Rev. Environ. Sci. Technol. **44**, 2502–2530 (2014). https://doi.org/10.1080/10643389.2013.829763
14. M. Suzuki, S. Sakuda, H. Nagasawa, Identification of chitin in the prismatic layer of the shell and a chitin synthase gene from the Japanese pearl oyster. Pinctada Fucata. Biosci. Biotechnol. Biochem. **71**, 1735–1744 (2007). https://doi.org/10.1271/bbb.70140
15. Y. Kong, G. Jing, Z. Yan, C. Li, N. Gong, F. Zhu, D. Li, Y. Zhang, G. Zheng, H. Wang, L. Xie, R. Zhang, Cloning and characterization of Prisilkin-39, a novel matrix protein serving a dual role in the prismatic layer formation from the oyster *Pinctada fucata*. J. Biol. Chem. **284**, 10841–10854 (2009). https://doi.org/10.1074/jbc.M808357200
16. R.A. Lutz, Bivalve Molluscs: biology, ecology and culture by Elizabeth Gosling. Q. Rev. Biol. **79**, 317 (2004). https://doi.org/10.1086/425799
17. L.J. De Nooijer, H.J. Spero, J. Erez, J. Bijma, G.J. Reichart, Biomineralization in Perforate Foraminifera. Earth-Sci. Rev. **135**, 48–58 (2014). https://doi.org/10.1016/j.earscirev.2014.03.013
18. S. Weiner, P.M. Dove, An overview of biomineralization processes and the problem of the vital effect. Rev. Mineral. Geochem. **54**, 1–29 (2003). https://doi.org/10.2113/0540001
19. B.R. Schöne, D.P. Gillikin, Unraveling environmental histories from skeletal diaries—advances in sclerochronology. Palaeogeogr. Palaeoclimatol. Palaeoecol. **373**, 1–5 (2013). https://doi.org/10.1016/j.palaeo.2012.11.026
20. J. Erez, The source of ions for biomineralization in Foraminifera and their implications for paleoceanographic proxies. Rev. Mineral. Geochem. **54**, 115–149 (2003). https://doi.org/10.2113/0540115
21. G.M. Henderson, New oceanic proxies for paleoclimate. Earth Planet. Sci. Lett. **203**, 1–13 (2002). https://doi.org/10.1016/S0012-821X(02)00809-9
22. M. Risk, M. Burchell, K. de Roo, R. Nairn, M. Tubrett, G. Försterra, Trace elements in bivalve shells from the Río Cruces, Chile. Aquat. Biol. **10**, 85–97 (2010). https://doi.org/10.3354/ab00268
23. J. Yu, H. Elderfield, B. Hönisch, B/Ca in planktonic foraminifera as a proxy for surface seawater pH. Paleoceanography **22**, PA2202 (2007). https://doi.org/10.1029/2006PA001347
24. J.E. Pietrzak, J.M. Bates, R.M. Scott, Constituents of unionoid extrapalial fluid. II. pH and metal ion composition. Hydrobiologia **50**, 89–93 (1976)
25. M. Zuykov, E. Pelletier, C. Belzile, S. Demers, Alteration of shell nacre micromorphology in blue mussel *Mytilus edulis* after exposure to free-ionic silver and silver nanoparticles. Chemosphere **84**, 701–706 (2011). https://doi.org/10.1016/j.chemosphere.2011.03.021
26. V. Yanko, A.J. Arnold, W.C. Parker, *Effects of Marine Pollution on Benthic Foraminifera—Modern Foraminifera* (Springer, Netherlands, Dordrecht, 2003)

27. R.J.P. Williams, J.J.R.F. da Silva, *The Natural Selection of the Chemical Elements* (Bath Press Ltd., Great Britian, 1996)
28. X.-M. Liu, L.C. Kah, A.H. Knoll, H. Cui, A.J. Kaufman, A. Shahar, R.M. Hazen, Tracing Earth's O_2 evolution using Zn/Fe ratios in marine carbonates. Geochemical Perspect. Lett. **2**, 24–34 (2016). https://doi.org/10.7185/geochemlet.1603
29. P.B. Tchounwou, C.G. Yedjou, A.K. Patlolla, D.J. Sutton, Heavy metal toxicity and the environment. Exp. Suppl. **101**, 133–164 (2012). https://doi.org/10.1007/978-3-7643-8340-4_6
30. R. Singh, N. Gautam, A. Mishra, R. Gupta, Heavy metals and living systems: An overview. Indian J. Pharmacol. **43**, 246–253 (2011). https://doi.org/10.4103/0253-7613.81505
31. D. Medas, I. Carlomagno, C. Meneghini, G. Aquilanti, T. Araki, D.E. Bedolla, C. Buosi, M.A. Casu, A. Gianoncelli, A.C. Kuncser, V.A. Maraloiu, G.D. Giudici, Zinc incorporation in marine bivalve shells grown in mine-polluted seabed sediments : a case study in the Malfidano mining area (SW Sardinia, Italy). Environ. Sci. Pollut. Res. (2018). https://doi.org/10.1007/s11356-018-3504-y
32. G. De Giudici, C. Meneghini, D. Medas, C. Buosi, P. Zuddas, A. Iadecola, O. Mathon, A. Cherchi, A.C. Kuncser, Coordination environment of Zn in foraminifera *Elphidium aculeatum* and *Quinqueloculina seminula* shells from a polluted site. Chem. Geol. **477**, 100–111 (2018). https://doi.org/10.1016/j.chemgeo.2017.12.009
33. T. Bechstädt, M. Boni, Sedimentological, stratigraphical and ore deposits field guide of the autochthonous Cambro-Ordovician of southwestern Sardinia: Servizio Geologico d'Italia Memorie Descritive Carta Geologica d'Italia, v. 48, 434 p. (1994)
34. A. Marcello, S. Pretti, P. Valera, M. Agus, M. Boni, M. Fiori, Metallogeny in Sardinia (Italy): from the Cambrian to the Tertiary, in *32nd International Geological Congress, APAT 4*, ed. by L. Guerrieri, L. Rischia, L. Serva, pp. 14–36, Firenze (2004)
35. M. Boni, H.A. Gilg, G. Aversa, G. Balassone, The "Calamine" of Southwest Sardinia: geology, mineralogy, and stable isotope geochemistry of supergene Zn mineralization. Econ. Geol. **98**, 731–748 (2003). https://doi.org/10.2113/gsecongeo.98.4.731
36. P. Stara, R. Rizzo, G.A. Tanca, Iglesiente-Arburese: Miniere e Minerali, Centrooffset, Siena (1996)
37. R. Bartole, S. De Muro, Acoustic facies and seabed features of the mixed carbonate-siliciclastic deposits of the last eustatic cycle in the La Maddalena Archipelago (North Sardinia, Italy). Ital. J. Geosci. **131**, 102–122 (2012). https://doi.org/10.3301/IJG.2011.28
38. M. Schintu, B. Marras, A. Maccioni, D. Puddu, P. Meloni, A. Contu, Monitoring of trace metals in coastal sediments from sites around Sardinia. Western Mediterranean. Mar. Pollut. Bull. **58**, 1577–1583 (2009). https://doi.org/10.1016/j.marpolbul.2009.07.015
39. V. Moschino, M. Schintu, A. Marrucci, B. Marras, N. Nesto, L. Da Ros, An ecotoxicological approach to evaluate the effects of tourism impacts in the Marine Protected Area of La Maddalena (Sardinia, Italy). Mar. Pollut. Bull. **122**, 306–315 (2017). https://doi.org/10.1016/j.marpolbul.2017.06.062
40. G. Salvi, C. Buosi, D. Arbulla, A. Cherchi, G. De Giudici, A. Ibba, S. De Muro, Ostracoda and foraminifera response to a contaminated environment: the case of the Ex-military arsenal of the la Maddalena Harbour (Sardinia, Italy). Micropaleontology **61**, 115–133 (2015)
41. W.R. Walton, Techniques for recognition of living foraminifera. Contrib. Cushman. Found. Foraminifer. Res. **3**, 56–60 (1952)
42. A.R. Loeblich Jr., H. Tappan, *Foraminiferal Genera and Their Classification* (Van Reinhold Company, New York, 1987)
43. F. Cimerman, M.R. Langer, Mediterranean Foraminifera. Ljubljana, Slovenska Akademija Znanosti in Umetnosti. Academia Scientiarum et ArtiumSlovencia Cl. 4 Historia Naturalis (1991)
44. L. Hottinger, E. Halicz, Z. Reiss, Recent Foraminiferida from the Gulf of Aqaba, Red Sea. Lubljana Academia Scientiarum et ArtiumSlovenica, Classis IV, Historia Naturalis (1993)
45. F. Sgarrella, M. Moncharmont Zei, Benthic foraminifera of the Gulf of Naples (Italy): systematics and autoecology. Boll. Soc. Paleontol. Ital. **32**, 145–264 (1993)

46. D.E. Conners, S.M. Westerfield, A. Feyko, M.C. Black, Lead Accumulation in soft tissues and shells of asiatic clams (*Corbicula fluminea*), in *The 1999 Georgia Water Resources Conference*, ed. by K. J. Hatcher, pp. 597–600 (1999)
47. A. Gianoncelli, G.R. Morrison, B. Kaulich, D. Bacescu, J. Kovac, Scanning transmission x-ray microscopy with a configurable detector. Appl. Phys. Lett. **89**, 251117–251119 (2006). https://doi.org/10.1063/1.2422908
48. G.R. Morrison, A. Gianoncelli, B. Kaulich, D. Bacescu, J. Kovac, A fast readout CCD system for configured-detector imaging in STXM, in *Proceedings of the 8th International Conference X-ray Microscopy. IPAP Conference Series*, pp. 277–379 (2006)
49. A. Gianoncelli, B. Kaulich, R. Alberti, T. Klatka, A. Longoni, A. de Marco, A. Marcello, M. Kiskinova, Simultaneous soft X-ray transmission and emission microscopy. Nucl. Instrum. Methods Phys. Res. Sect. A Accel. Spectrometers, Detect. Assoc. Equip. **608**, 195–198 (2009). https://doi.org/10.1016/j.nima.2009.06.035
50. A. Gianoncelli, G. Kourousias, A. Stolfa, B. Kaulich, Recent developments at the TwinMic beamline at ELETTRA: an 8 SDD detector setup for low energy X-ray Fluorescence. J. Phys. Conf. Ser. **425**, 182001 (2013). https://doi.org/10.1088/1742-6596/425/18/182001
51. A. Gianoncelli, G. Kourousias, L. Merolle, M. Altissimo, A. Bianco, Current status of the TwinMic beamline at Elettra: a soft X-ray transmission and emission microscopy station. J. Synchrotron Radiat. **23**, 1526–1537 (2016). https://doi.org/10.1107/S1600577516014405
52. A. Gianoncelli, G. Kourousias, M. Altissimo, D.E. Bedolla, L. Merolle, A. Stolfa, H.-J. Shin, Combining multiple imaging techniques at the TwinMic X-ray microscopy beamline. AIP Conf. Proc. **1764**, 30002 (2016). https://doi.org/10.1063/1.4961136
53. B. Kaulich, D. Bacescu, J. Susini, C. David, E. Di Fabrizio, G.R. Morrison, P. Charalambous, J. Thieme, T. Wilhein, J. Kovac, D. Cocco, M. Salome, O. Dhez, T. Weitkamp, S. Cabrini, D. Cojoc, A. Gianoncelli, U. Vogt, M. Podnar, M. Zangrando, M. Zacchigna, M. Kiskinova, *Proceeding 8th International Conference X-ray Microscopy IPAP Conference Series*. Presented at the (2006)
54. Numpy: https://docs.scipy.org/doc/numpy-1.14.0/reference/generated/numpy.corrcoef.html. Copyright 2008–2009, The Scipy community. Last updated on 11 May 2014
55. scipy: https://docs.scipy.org/doc/scipy-0.14.0/reference/generated/scipy.stats.spearmanr.html. Copyright 2008–2009, The Scipy community. Last updated on 11 May 2014
56. A. Di Cicco, G. Aquilanti, M. Minicucci, E. Principi, N. Novello, A. Cognigni, L. Olivi, Novel XAFS capabilities at ELETTRA synchrotron light source. J. Phys. Conf. Ser. **190**, 12043 (2009). https://doi.org/10.1088/1742-6596/190/1/012043
57. M. Benfatto, C. Meneghini, A close look into the low energy region of the XAS spectra: the XANES region, in *Synchrotron Radiation, Basic, Methods and Applications*, ed. by S. Mobilio, F. Boscherini, C. Meneghini (Springer-Verlag, Berlin, 2014), pp. 213–240
58. R. Torchio, C. Meneghini, S. Mobilio, G. Capellini, A. Garcia Prieto, J. Alonso, M.L. Fdez-Gubieda, V. Turco Liveri, A. Longo, A.M. Ruggirello, T. Neisius, Microstructure and magnetic properties of colloidal cobalt nano-clusters. J. Magn. Magn. Mater. **322**, 3565–3571 (2010). https://doi.org/10.1016/j.jmmm.2010.07.008
59. C. Meneghini, F. Bardelli, S. Mobilio, ESTRA-FitEXA: a software package for EXAFS data analysis. Nucl. Instrum. Methods Phys. Res. Sect. B Beam Interact. Mater. Atoms. **285**, 153–157 (2012). https://doi.org/10.1016/j.nimb.2012.05.027
60. O. Mathon, A. Beteva, J. Borrel, D. Bugnazet, S. Gatla, R. Hino, I. Kantor, T. Mairs, M. Munoz, S. Pasternak, F. Perrin, S. Pascarelli, The time-resolved and extreme conditions XAS (TEXAS) facility at the European Synchrotron Radiation Facility: the general-purpose EXAFS bending-magnet beamline BM23. J. Synchrotron Radiat. **22**, 1548–1554 (2015). https://doi.org/10.1107/S1600577515017786
61. C.K. Carney, S.R. Harry, S.L. Sewell, Detoxification biominerals, in *Biomineralization I. Topics in Current Chemistry*, ed. by K. Naka (Springer, Berlin, Heidelberg, 2007), pp. 155–185
62. V. Le Cadre, J.-P. Debenay, Morphological and cytological responses of Ammonia (foraminifera) to copper contamination: implication for the use of foraminifera as bioindicators of pollution. Environ. Pollut. **143**, 304–317 (2006). https://doi.org/10.1016/j.envpol.2005.11.033